Multiple cross-correlation staining reverse time migration for high-resolution fracture imaging

Congcong Yuan, Xiaofeng Jia, Shishuo Liu, Jie Zhang, University of Science and Technology of China (USTC)*

Summary

Accurate characterization of hydraulic fracturing zones is currently becoming more and more important in production optimization, because such fractures may increase the porosity and permeability of the reservoirs significantly. Recently, reverse time migration (RTM) has been applied for fracture imaging during borehole microseismic monitoring. However, strong low-frequency migration noise, poorly illuminated areas, and low signal to noise ratio (SNR) of data lead to poor imaging results. To improve the quality of imaging, we introduce the staining algorithm and propose a multiple cross-correlation imaging condition and apply them to microseismic fracture imaging with scattering data. Our results show that, compared with conventional RTM, the spatial resolution of imaging is improved significantly.

Introduction

Scattered waves from subsurface fractures have been widely applied in microseismic monitoring field. A variety of methods are designed to estimate the parameters of fractures with them. For unconventional reservoirs with passive seismic sources, Maxwell et al. (2010) reveal that microseismic events distributed around fractures could provide insight into fracture parameters, including location, height, length, orientation, and complexity.

Recently, concepts of exploration seismology are adapted to image structure discontinuities at various scales using scattered waves (Chavarria et al., 2003; Zhang et al., 2009; Reshetnikov et al., 2010a and 2010b; Lin et al., 2016). Due to its capability of handling different kinds of wavefields, reverse time migration (RTM) is more suitable for imaging complicated structures, compared with methods such as Kirchhoff migration (Shneider, 1978), beam migration (Hill, 1990), one-way wave-equation migration (Claerbout, 1971), etc. Our work is focused on improvement of spatial resolution of RTM to obtain more accurate description of fractures in hydraulic treatment.

We propose the method of multiple cross-correlation staining reverse time migration (MCSRTM) in this study. It is first presented by Chen and Jia (2014), that if a certain structure in the velocity model is stained, the passing wave will also be stained and thus can be identified and tracked in subsequent propagation. The staining algorithm labels a certain structure and generates a wavefield and data that are exclusively related to the structure. The method shows its advantages in coping with poorly-illuminated area, such as sub-salt structure, the wave from which are distorted strongly by the salt bodies. We introduce the method to microseismic fracture imaging to improve the spatial resolution and suppress the distortion and smearing effects caused by low frequency noise and cross-talk between the scattered waves from adjacent fractures.

Stained wavefield and stained data

"Stained wavefield" refers to the wavefield triggered by the stained target structure, which is a subset of the full wavefield. In wave propagation, only when a wave reaches the target structure is it labeled and the stained wavefield (synchronized with the conventional wavefield) triggered. The stained wavefield represents the propagation of the energy related to the target structure, which is useful for investigating the characteristics of fractures. We adopt the generalized staining algorithm (GSA) (Li and Jia, 2016) in our study to take its advantage of amplitude preservation. The wave equations for the real and stained wavefields are given as

$$\frac{\partial^2 \bar{p}}{\partial t^2} = \bar{v}^2 \Delta \bar{p} + \bar{s} \tag{1}$$

$$\frac{\partial^2 \tilde{p}}{\partial t^2} = \bar{v}^2 \Delta \tilde{p} \tag{2}$$

$$\tilde{p}\,|_{D=1} = \bar{p} \tag{3}$$

$$D = \begin{cases} 1, & stained \\ 0, & elsewhere \end{cases} \tag{4}$$

In the equations, $\bar{p}$ and $\tilde{p}$ refer to real and stained wavefields, while $\bar{v}$ and $\bar{s}$ represent the velocity and the source. D labels the stained boundary, where the stained wavefield is linked to the real wavefield as boundary condition. The Kirchhoff integral (Wiggins, 1984; Docherty, 1991) gives the solution to equation (1) as:

$$\frac{1}{4\pi}\int d\tau \oint_{D=1} (G(\vec{r};\vec{r}'',t,\tau)\frac{\partial \bar{p}(\vec{r}'',\tau)}{\partial n} - \bar{p}(\vec{r}'',\tau)\frac{\partial G(\vec{r};\vec{r}'',t,\tau)}{\partial n})dS$$
$$-\int d\tau \iiint_{V^c} \bar{s}(\vec{r}',\tau)G(\vec{r};\vec{r}',t,\tau)d\vec{r}'^3 = 0 \tag{5}$$

$$\bar{p}(\vec{r},t) = \frac{1}{4\pi}\int d\tau \iiint_{V^c} \bar{s}(\vec{r}', \quad \tau)G(\vec{r};\vec{r}',t,\tau)d\vec{r}'^3 \tag{6}$$

We can rebuild the real wavefield inside a closed stained boundary by implementing the Kirchhoff Integral on it. Because the integral of far field has trivial influence on the result, we can stain part of the boundary instead. Hence, by linking the value of stained wavefield to real wavefield at $D=1$, we can calculate the forward-propagating stained wavefield, which is approximately the same in amplitude as the real wavefield which passes the stained boundary. The workflow is given in Figure 1 with the left part showing the GSA implementation.

Imaging Condition

In conventional RTM, the imaging condition is the cross-correlation of source wavefield and receiver wavefield, presented as follows:

$$I(\vec{r}) = \int_t s(\vec{r},t)w(\vec{r},t)dt \tag{7}$$

s refers to the forward propagating source wavefield, while w stands for the backward propagating receiver wavefield. We can apply equation (7) to both real and stained wavefields to obtain corresponding seismic images, shown as

$$I_{real}(\vec{r}) = \int_t s_{real}(\vec{r},t)w(\vec{r},t)dt \tag{8}$$

$$I_{stained}(\vec{r}) = \int_t s_{stained}(\vec{r},t)w(\vec{r},t)dt \tag{9}$$

Inspired by the method of GmRTM proposed by Nakata and Beroza (2016), we attempt to introduce the concept of multiple cross-correlation to our development of the imaging condition.

Nakata and Beroza's method (2016) is based on the concept of seismic interferometry, as shown in Figure 2(a), the data of receivers r_i and r_j are back propagated individually as the wavefields of $w_i(\vec{r},t)$ and $w_j(\vec{r},t)$. After conducting a zero-time-shift cross-correlation, the location of scatterer (or passive source) is obtained. Extending the cross-correlation to all receivers, they obtain the image of scatterer (or passive source) shown as:

$$I(\vec{r}) = \sum_t \prod_i w_i(\vec{r},t) \tag{10}$$

It can be regarded as the focusing of wavefields of different receivers.

Considering our situation, we need to recover the image of scattering fractures from the scattering data and the stained source wavefield, which is illustrated in Figure 2(b).

Suppressing low-frequency noise and reducing artifacts are the primary consideration to us. Note that the noise and artifacts in imaging are highly relevant to the distribution of receivers. If we obtain the image of each receiver independently and conduct an accumulative multiplication, similar to (but different from) equation (10), noises and artifacts varying with the location of receivers can be effectively removed and the final image shall be focused. The method is implemented in five steps as follows:

(1) Divide the total N-receiver array into different groups according to their spatial distribution, assuming that each group has the same number of receivers n.

(2) Backward propagate scattering data of different groups individually and obtain the corresponding scattering wavefield $w_i(\vec{r},t)$, $(i=1,2,...,N/n)$.

(3) Conduct forward propagation using source information. Staining algorithm is applied to obtain real forward wavefield $s_{\text{real}}(\vec{r},t)$ and stained wavefield $s_{stained}(\vec{r},t)$.

(4) Cross-correlate the forward wavefield and scattered wavefield of each receiver group, respectively, and obtain the images of different groups:

$$\overline{M}_i(\vec{r}) = \int_t s_{real}(\vec{r},t)w_i(\vec{r},t)dt \tag{11}$$

$$\widetilde{M}_i(\vec{r}) = \int_t s_{stained}(\vec{r},t)w_i(\vec{r},t)dt \tag{12}$$

(5) Apply accumulative multiplication to the images of all groups, and the final images are given by

$$I_{real}(\vec{r}) = \prod_{i=1}^{N/n} \overline{M}(\vec{r}) \tag{13}$$

$$I_{stained}(\vec{r}) = \prod_{i=1}^{N/n} \widetilde{M}(\vec{r}) \tag{14}$$

The full workflow of our method is shown in Figure 1, with the GSA steps in the left part, while the multiple cross-correlation imaging condition in the right part.

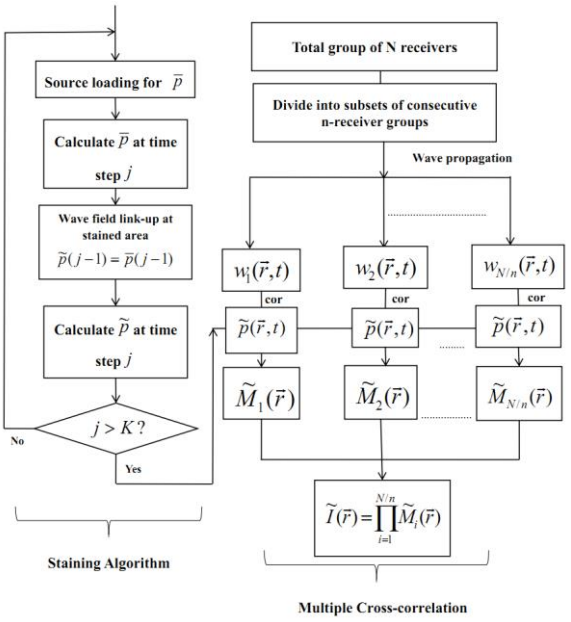

Figure 1: Workflow chart of our imaging method, with GSA in the left part, where K is the step number of iteration. And the receiver wavefield propagation with imaging condition shown on the right.

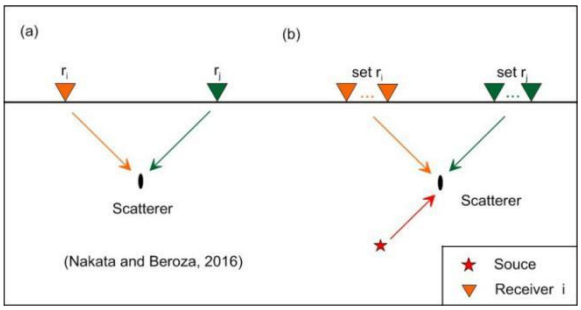

Figure 2: Scattering wavefield from an embedded fracture.

Numerical Examples

Our numerical experiments are conducted on a layer velocity model with a simple survey geometry of a microseismic event and a vertical receiver array. As shown in Figure 3(a), the velocity model includes three layers of values 3.0, 3.5 and 4.0 km/s, with the white star representing the microseismic source and the black triangles standing for the receiver array. If we apply GSA and set D =1 (staining mark) on the vertical line at 0.9 km horizontal position in Figure 3(b), we can obtain the real wavefield in Figure 3(c), and staining wavefield in Figure 3(d) after 0.1 second of wave propagation from the source.

In the experiments we set 3 embedded fractures in the layered model, shown in Figure 4(a). The receiver data we adopt is scattering data from the fractures simulated by a hybrid method proposed by Li et al (2011), shown in Figure 4(b). To improve the spatial resolution of the fracture area, we apply two staining schemes, the first is a straight line between the left fracture and the middle one, shown as Figure 5(a), and the second is a straight line of the same length between the middle and right fractures, shown as Figure 5(b).

We start our imaging tests with conventional RTM. The result is shown in Figure 6(a). The locations of the fractures are roughly indicated on the image, with relatively strong low-frequency noise as well as arc shaped artifacts. With staining algorithm implemented, we obtain the images of Figure 6(c) and Figure 6(e). We can observe that the irrelevant energy (especially the background low-frequency noise) is effectively suppressed compared with Figure 6(a). However, the artifacts on the left of receivers still exist.

To further improve the resolution of our images and reduce the artifacts, we adopt the multiple cross-correlation imaging condition as the final step of our imaging workflow. The images in Figure 6(b), 6(d) and 6(f) show the results of multiple cross-correlation imaging condition of corresponding staining schemes in Figure 6(a), 6(c) and 6(e). We can observe that the images are considerably sharper and with more accurate fracture locations indicated.

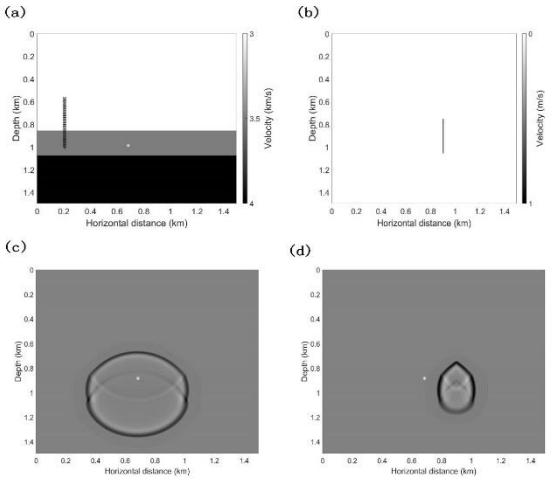

Figure 3: Velocity model with stained area and corresponding snapshots of the real and stained wavefields at 0.1 s.

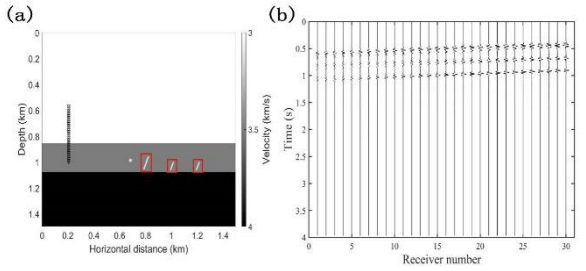

Figure 4: Fracture model and scattering data. (a) The real velocity model corresponding to Figure 3(a) with three fractures marked by the red boxes. (b) The recordings on the receiver array from the microseismic event.

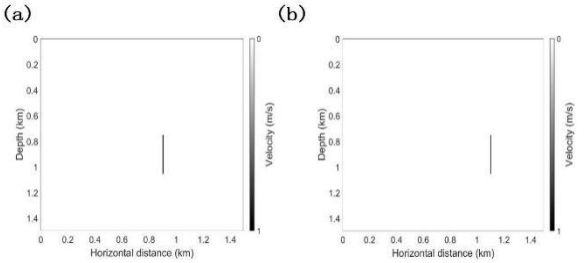

Figure 5: Two staining schemes at corresponding positions: (a) The first scheme on the line between the left and middle fractures. (b) The second staining scheme on the line between the middle and right fractures.

Conclusions

We propose the method of MCSRTM for improving the spatial resolution of fracture imaging in microseismic monitoring field. The method extracts the wavefield relevant to the target fractures with proper staining schemes, and significantly reduce low frequency noise and artifacts. Its feasibility of fracture imaging is promising for optimization of reservoir recovery industry. The effects of location uncertainty and velocity inaccuracy will be considered and analyzed on the imaging results in our further study.

Acknowledgements

We gratefully acknowledge the financial support of the National Natural Science Foundation of China (Grant No.41374132 & 41374006). We appreciate the support from Dr. Junlun Li, allowing us to utilize the scattered wave modeling code to perform this study. We are also thankful to Bo Chen and Qihua Li for suggestions and sharing the staining code.

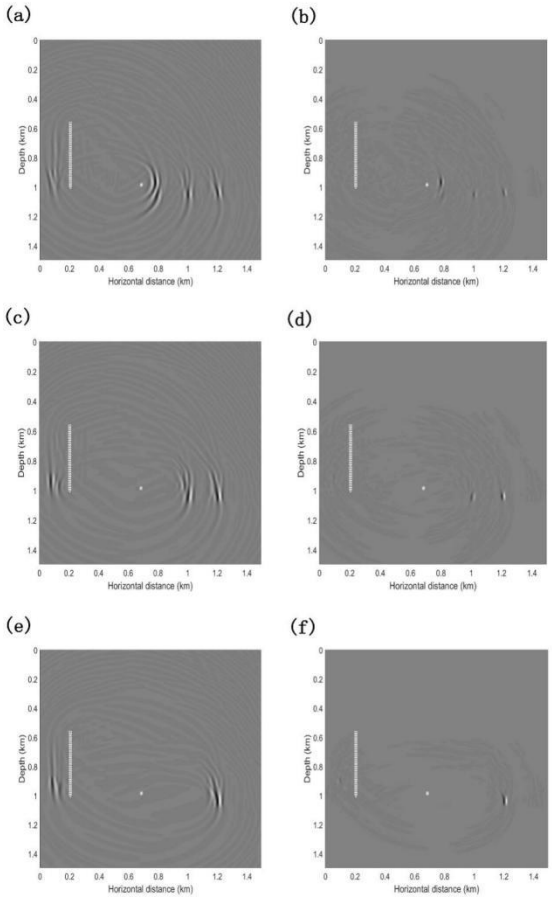

Figure 6: The left three images are imaged with (a) non stained model (conventional RTM), (c) first stained scheme, and (e) second stained scheme by using conventional RTM with staining algorithm. Other three images are corresponding to the left ones with multiple cross-correlation imaging condition. The white star and reverse triangles are microseismic event and receivers, respectively.